EPJ manuscript No.
(will be inserted by the editor)

Smearing origin of zero-bias conductance peak in Ag–SiO–$Bi_2Sr_2CaCu_2O_{8+\delta}$ planar tunnel junctions: influence of diffusive normal metal verified with the circuit theory

Iduru Shigeta[1,a], Yukio Tanaka[2,3], Fusao Ichikawa[4], and Yasuhiro Asano[5]

[1] Department of General Education, Kumamoto National College of Technology, Kumamoto 861-1102, Japan
[2] Department of Applied Physics, Nagoya University, Nagoya 464-8603, Japan
[3] CREST, Japan Science and Technology Agency (JST), Nagoya 464-8603, Japan
[4] Department of Physics, Kumamoto University, Kumamoto 860-8555, Japan
[5] Department of Applied Physics, Hokkaido University, Sapporo 060-8628, Japan

Received 25 January 2006 / Received in final form 23 October 2006

Abstract. We propose a new approach of smearing origins of a zero-bias conductance peak (ZBCP) in high-T_c superconductor tunnel junctions through the analysis based on the circuit theory for a d-wave pairing symmetry. The circuit theory has been recently developed from conventional superconductors to unconventional superconductors. The ZBCP frequently appears in line shapes for this theory, in which the total resistance was constructed by taking account of the effects between a d-wave superconductor and a diffusive normal metal (DN) at a junction interface, including the midgap Andreev resonant states (MARS), the coherent Andreev reflection (CAR) and the proximity effect. Therefore, we have analyzed experimental spectra with the ZBCP of Ag–SiO–$Bi_2Sr_2CaCu_2O_{8+\delta}$ (Bi-2212) planar tunnel junctions for the {110}-oriented direction by using a simplified formula of the circuit theory for d-wave superconductors. The fitting results reveal that the spectral features of the ZBCP are well explained by the circuit theory not only excluding the Dynes's broadening factor but also considering only the MARS and the DN resistance. Thus, the ZBCP behaviors are understood to be consistent with those of recent studies on the circuit theory extended to the systems containing d-wave superconductor tunnel junctions.

PACS. 74.25.Fy Transport properties (electric and thermal conductivity, thermoelectric effects, etc.) – 74.45.+c Proximity effects; Andreev effect; SN and SNS junctions – 74.50.+r Tunneling phenomena; point contacts, weak links, Josephson effects – 74.72.Hs Bi-based cuprates

1 Introduction

The experimental studies of zero-bias conductance peak (ZBCP) behaviors have been frequently reported for various unconventional superconductors with an anisotropic pairing symmetry, for instance, p-wave and d-wave pairing symmetries [1–17]. The ZBCP that results from the Anderson-Appelbaum scattering has been studied thoroughly via previous experiments [18–22]. However, only until recently was there an alternate theory to explain the origin of the ZBCP. In this theory, the ZBCP has been understood as the formation of the midgap Andreev resonant states (MARS) at a junction interface in a ballistic normal metal–insulator–superconductor (N/I/S) tunnel junction [23]. A basic theory of ballistic transport in the presence of the MARS has been formulated in the case of d-wave superconductors by way of the Blonder-Tinkham-Klapwijk (BTK) theory [24]. This model has sufficiently explained ZBCP behaviors in high-T_c cuprate superconductors. Another mechanism of the ZBCP plays a role in the coherent Andreev reflection (CAR), which induces the proximity effect in the diffusive normal metal (DN) [25] at a diffusive normal metal–insulator–superconductor (DN/I/S) junction interface. Then, there are two kinds of the ZBCP due to the formation of the MARS at junction interfaces of d-wave superconductors and of that due to the CAR by the proximity effect in the DN.

The circuit theory includes both effects of the MARS and the CAR due to constructing the theory at a junction interface under the condition of DN/I/S tunnel junctions for s-wave, p-wave and d-wave superconductors [26–34]. Figure 1(a) illustrates the schematic drawing at a junction interface of a $d_{x^2-y^2}$-wave superconductor for the circuit theory. In this theory, the ZBCP frequently appears in the line shapes of normalized tunneling conductance $\sigma_{\rm T}(eV)$, and we always expect the ZBCP to be independent of α for low transparent junctions with the small Thouless energy $E_{\rm Th}$. Here, $\sigma_{\rm T}(eV)$ is defined as dividing tunnel-

[a] *Present address:* Department of Physics, Kagoshima University, Kagoshima 890-0065, Japan.

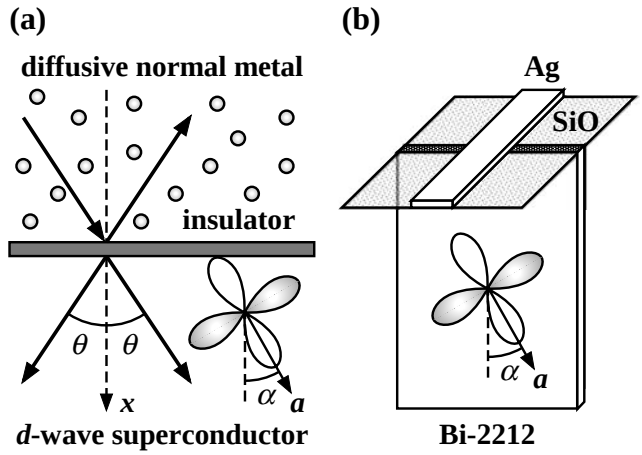

Fig. 1. (a) Schematic illustration of incoming and outgoing processes at the junction interface for the diffusive normal metal–insulator–unconventional superconductor tunnel junction. The unconventional superconductor junctions can be incorporated into the circuit theory by means of the relation between matrix current and asymptotic Green's functions [28]. This relation accounts for anisotropic features of the *d*-wave superconductors, as sketched for a *d*-wave superconductor. (b) Planar type junction layout for the *ab*-plane direction. The Ag–SiO–Bi-2212 planar tunnel junction contains the SiO layer between the Ag thin film of the counterelectrode and the Bi-2212 single crystal enclosed with epoxy resin. The SiO barrier and Ag counterelectrode are deposited perpendicular to the *ab*-plane of Bi-2212 single crystals.

ing conductance $\sigma_{\rm S}(eV)$ in the superconducting state by tunneling conductance $\sigma_{\rm N}(eV)$ in the normal state, and α denotes the angle between the normal to the interface and the crystal axis of *d*-wave superconductors. The nature of the ZBCP due to the MARS and that due to the CAR are significantly different. The corresponding $\sigma_{\rm T}(0)$ for the former case can take arbitrary values exceeding unity. On the other hand, $\sigma_{\rm T}(0)$ for the latter case never exceeds unity. Furthermore, the the ZBCP width in the former case is determined by the transparency of the junction, while the width in the latter case is determined by $E_{\rm Th}$. These two ZBCPs compete with each other since the proximity effect and the existence of the MARS are incompatible in singlet junctions.

The influence of the resistance $R_{\rm d}$ in a DN is significant for the resulting $\sigma_{\rm T}(eV)$. Hence, for the actual quantitative comparison with tunneling experiments, we must take into account the effect of $R_{\rm d}$. In the circuit theory for *d*-wave superconductors, the ZBCP is frequently seen in the line shapes of $\sigma_{\rm T}(eV)$. For $\alpha = 0$, the ZBCP is due to the CAR. However, for $\alpha \neq 0$, the robustness of the ZBCP does not depend on the DN resistance $R_{\rm d}$. In such an extreme case as $\alpha = \pi/4$, the ZBCP arises from the MARS, and the CAR and the proximity effect are absent. The $\sigma_{\rm T}(eV)$ is then given by an elementary application of Ohm's law: $\sigma_{\rm T}(eV) = (R_{\rm b} + R_{\rm d})/(R_{R_{\rm d}=0} + R_{\rm d})$ [28,30], where $R_{\rm b}$ is the resistance from the insulating barrier in a normal state and $R_{R_{\rm d}=0}$ is the total resistance of the DN/I/S tunnel junction in the condition of $R_{\rm d} = 0$. In the case of $R_{\rm d} = 0$, there is no proximity effect in the DN, and the junction resistances are given by the quasiballistic formulas of ref. [23]. Therefore, the theoretical results serve as an important guide to analyzing the actual experimental data of the tunneling spectra of high-$T_{\rm c}$ cuprate junctions.

In the present paper, we will discuss the ZBCP behaviors in Ag–SiO–$Bi_2Sr_2CaCu_2O_{8+\delta}$ (Bi-2212) planar tunnel junctions by using the circuit theory for $d_{x^2-y^2}$-wave superconductors in the case of $\alpha = \pi/4$, and then, for analysis of the ZBCP, we will focus on the MARS case involving an influence of $R_{\rm d}$, not the CAR or the proximity effect cases.

2 Experimental details

Planar type tunnel junctions are fabricated in some experiments, while other measurements rely on scanning tunneling microscopy and spectroscopy (STM/STS) for recent spectroscopic purposes. The STM/STS has the advantages of versatility adjustable junction resistance, simultaneous topographical imaging at atomic scale resolutions together with the spatial variations of local density of states (LDOS), and momentum space ($\boldsymbol{k}$-space) images obtained by Fourier transformation of real space ($\boldsymbol{r}$-space) informations [35–42]. However, it suffers from a lack of stability against temperature and magnetic field changes, so a planar tunnel junction is a more suitable device for temperature and magnetic field dependence studies. Most ZBCP studies are on $YBa_2Cu_3O_{7-\delta}$ (Y-123) thin film in planar tunnel junction experiments [43–46]. Some of these films are highly oriented, thereby making the study on angular dependence of ZBCPs possible [47]. However, we chose to use Bi-2212 single crystals in tunneling spectroscopic measurements, nevertheless, as the ZBCP is not commonly available or studied on such mediums as Y-123. Bi-2212 has several advantages in terms of properties rather than other high-$T_{\rm c}$ cuprates. For example, Bi-2212 is very stable against losing oxygen, retains a cleavage property between BiO planes, possesses a large anisotropy ratio between the *ab*-plane and *c*-axis directions, and its single crystal does not twin like Y-123.

Bi-2212 single crystals were prepared by the traveling solvent floating-zone (TSFZ) method, and the superconducting transition temperature $T_{\rm c}$ of each as-grown single crystal was 87–90 K, which was decided by the resistivity and magnetic susceptibility measurements. For hole doping concentration, as-grown single crystals are located on slightly overdoped regions in the critical temperature-doping phase diagram [48]. We have prepared planar tunnel junctions by using these single crystals. Figure 1(b) shows a layout of a planar tunnel junction for the *ab*-plane directions. A single crystal with a size of approximately 10 mm × 3 mm × 50 μm was molded into a block of epoxy resin. The block of epoxy resin was cut to expose the {110}-oriented surface of the single crystals. This cut surface was polished roughly by sandpaper, then smoothed by diamond pastes with lubricant in the further process.

At that point, SiO was evaporated normal on the {110}-oriented surface as a insulating barrier, and the thickness of SiO layer was modified between 0 Å and 300 Å for each planar tunnel junction. Ag was deposited on the SiO thin film through a metal mask patterned with a counterelectrode of strips with width of 0.5 mm. The thickness of the Ag layer was controlled to be 1500 Å. For the planar type junctions made in this manner, Au wires were attached to the Ag thin film with Ag paste, where the length L between the cross section of the tunnel junction and Ag paste regarded as the reservoir in the circuit theory is roughly 1–2 mm. The total number of measured samples was more than 50. In our experiments, the crystal orientation at the junction interface, expressed as α in Figs. 1(a) and 1(b), could be predetermined from a sample rod configuration fabricated by the TSFZ method since the sample rod grows up to the a-axis direction of Bi-2212 single crystals in this method. This fact was confirmed by taking into account the satellite reflections arising from an incommensurate modulated structure in the X-ray diffraction pattern of Bi-2212 single crystals [49,50].

We have collected I–V and $\mathrm{d}I/\mathrm{d}V$–V data for the prepared planar tunnel junctions by the standard 4-terminal method. The $\mathrm{d}I/\mathrm{d}V$–V data corresponding to $\sigma_{\mathrm{T}}(eV)$ were measured by using the conventional voltage modulation method. The temperature ranged from 4.2 K to 300 K, using a temperature controller with a stability of more than 0.1 K. Al–Al_2O_3–Pb planar tunnel junctions were fabricated and their tunneling spectra were measured in advance, in order to compare differences about the pairing symmetry of the superconducting order parameter between conventional superconductors and high-T_{c} cuprate superconductors.

3 Results and discussion

3.1 Tunneling conductance measurements

We have measured tunneling spectra of Ag–SiO–Bi-2212 planar tunnel junctions. Figure 2 represents typical tunneling conductance $\sigma_{\mathrm{S}}(eV)$ of the ZBCP in the superconducting state, which was obtained on several {110}-oriented tunnel junctions. SiO thin films as tunnel barrier become gradually thicker from Fig. 2(a) to Fig. 2(c). The values of tunneling conductance tend to enlarge with decreasing thickness of the SiO barrier, but we cannot verify the definite dependence of the ZBCP height on the insulating barrier thickness. Then, there is no large difference between the {110}-oriented tunnel junctions for concerning spectral shapes of the ZBCP, which was observed in most of our planar tunnel junctions. The ZBCP had a peak height of 2.0–3.3 times higher than the background and a full-width at half maximum (FWHM) of 3.3–6.5 meV in our experiments. For the tunnel junctions that display the ZBCP, many peaks are higher and sharper than the limit allowed by the BTK theory. This ZBCP enhancement clearly indicates an intrinsic property of the d-wave pairing symmetry in singlet superconductors. As shown in Fig. 2, both sides of the background around the

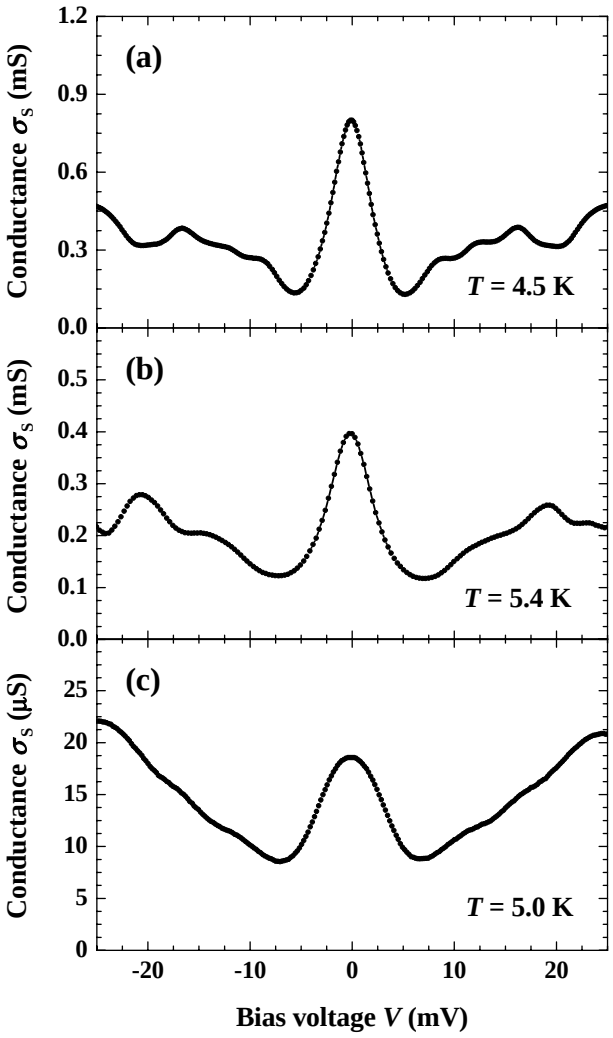

Fig. 2. Comparison of typical spectral shapes for tunneling conductance $\sigma_{\mathrm{S}}(eV)$ in the several {110}-oriented tunnel junctions. An enhancement of the reproducible ZBCP was frequently observed below T_{c} in most of planar tunnel junctions for the {110}-oriented direction. There are the dip and weak modulation structures at the outside of the ZBCP.

ZBCP gradually increase with leaving zero-bias voltage and have weak modulation structures. We conceive that the weak modulation structures appeared by the specific current-path effect, due to the slight surface roughness at the junction interface [9]. The coherent peaks at an energy gap region and any other specific structures are not observed in tunneling conductance except for the ZBCP.

On the other hand, the typical $\sigma_{\mathrm{T}}(eV)$ tunneling into the {001}-oriented surface, which was the cleavage surface of Bi-2212 single crystals, had a well-known V-shaped gap structure [51]. The d-wave pairing symmetry of an order parameter is evidently suggested from an anisotropy of the tunneling spectra, such as the V-shaped gap structure in the {001}-oriented direction and the ZBCP in the {110}-oriented direction. In contrast to Ag–SiO–Bi-2212 planar tunnel junctions, a U-shaped gap structure with an en-

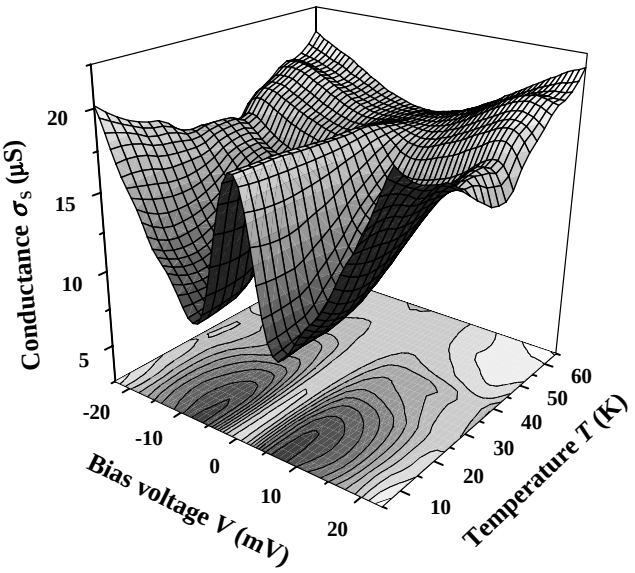

Fig. 3. Temperature dependence of the ZBCP for the {110}-oriented tunnel junction in Fig. 2(c). When the temperature decreased, the ZBCP height increased, the ZBCP width sharpened, and the weak modulation structures enlarged. The ZBCP appeared below roughly $T = 60$ K.

ergy gap $\Delta_0 \simeq 1.4$ meV was observed for Al–Al_2O_3–Pb planar tunnel junctions at $T = 1.8$ K, where Pb was a superconducting state and Al was a normal state. These tunnel junctions preserved resistances of more than several thousand ohms, so we consider that said junctions correspond to ranges for high potential barrier height as the Bardeen-Cooper-Schrieffer (BCS) limit in the BTK theory, in which a tunneling spectral shape expects the U-shape gap structure for *s*-wave superconductors.

Figure 3 represents the temperature dependence of the ZBCP for the {110}-oriented tunnel junction in Fig. 2(c). When the temperature decreased, the ZBCP height enlarged, the ZBCP width sharpened, the dip grew outside around the ZBCP, and the weak modulation structures appeared around the ZBCP. As shown in Fig. 3, the ZBCP appeared below roughly 60 K. In our tunneling experiments, the ZBCP appeared at T_c for several tunnel junctions and below T_c for the other tunnel junctions with the decrease in temperature. Hence, the experimental results of the temperature dependence also denote that the ZBCP is obviously caused by superconductivity.

Here, we will discuss other possible origins of the ZBCP in tunneling conductance; for example, the magnetic impurity effect, known as the Anderson-Appelbaum model taking account of the *s*-*d* exchange interaction [18–20], near the junction interface. However, the possibility of the magnetic impurity effect is strongly contradicted because the ZBCP enhancement has not been measured in the {001}-oriented direction, of which the tunnel junctions were also fabricated by using the same materials and procedures as those of the {110}-oriented direction, as described in sec. 2. Moreover, the ZBCP has been observed only below T_c. These facts obviously show that the ZBCP comes from not the magnetic impurity effect, but the superconductivity of the *d*-wave pairing symmetry. Thus, the experimental results in Figs. 2 and 3 coincide with the expectation of the MARS theory for *d*-wave superconductors. Furthermore, we will compare our experimental results with previous research on planar tunnel junctions for Bi-2212 single crystals [17]. S. Sinha *et al.* reported that the ZBCP enhanced in *ab*-plane directions at liquid-helium temperatures and disappeared above T_c with increasing temperature [52,53]. Their experimental results of the ZBCP behaviors are similar to ours nevertheless the tunneling direction in the *ab*-plane at the junction interface was not controlled in their experiments.

Another problem for the ZBCP remains, regarding the broken time-reversal symmetry (BTRS) at a junction interface of anisotropic superconductors [54–56]. The ZBCP must split below T_c if the BTRS occurs at the SIN junction interface. However, as shown in Figs. 2 and 3, there is no ZBCP splitting in all of the planar tunnel junctions for the {110}-oriented direction, on the condition of temperature ranges of 4.2–300 K not applied to magnetic fields. Thus, we have deduced that the BTRS does not occur at the high-T_c superconductor junction interface from our experiments.

3.2 Application to the circuit theory

We will here discuss the smearing origin from a different point of view against two theoretical analyses on the experimental ZBCP. The actual ZBCP height depends on smearing processes of several possible sources. One of these substantial smearing effects is due to the increase in the number of quasiparticles owing to thermal excitation. Although the tunnel junctions were studied at relatively low temperatures ($T/T_c \simeq 0.06$, in the case of $T = 5.0$ K) to minimize the effect of thermal excitations and to allow a more straightforward deconvolution of the ZBCP structure, the ZBCP height was not very high, when compared to the expectation of the ballistic theory including the MARS mechanism [23]. In most of previous research, the origin of smearing processes was usually explained as a result of the finite lifetime of quasiparticles in superconductors by introducing the broadening factor Γ, where E is replaced by $E - i\Gamma$ using the Dynes's method in formulas of tunneling spectra [57,58]. Here, the Dynes's parameter Γ is introduced phenomenologically; accordingly this method has not made clear how and where the finite lifetime of quasiparticles comes from specifically. However, this could be achieved to elucidate tunneling spectral behaviors, sometimes even under changing temperatures or magnetic fields, then used to fit theoretical curves of tunneling spectral formulas with many experimental tunneling spectra up to the present [59–69].

Up to this point, our experimental results for Ag–SiO–Bi-2212 planar tunnel junctions reveal that Bi-2212 is evidently a *d*-wave superconductor and that the ZBCP for {110}-oriented tunnel junctions obviously arises from superconductivity. We adapt the $d_{x^2-y^2}$-wave pairing sym-

metry for an order parameter of Cooper pairs in Bi-2212 compounds for the analysis of the circuit theory, because of the experimental evidence for many other results in several measurement methods [70–74], as well as for the ZBCP enhancement of the {110}-oriented direction in our tunneling spectroscopic measurements. Here, we choose $\alpha = \pi/4$ as the orientation of Bi-2212 single crystals at the junction interface, since the {110}-oriented surfaces were exposed at each junction interface as shown in Figs. 2 and 3. For $\alpha = \pi/4$ the CAR and the proximity effect are completely suppressed and only the MARS remain, while for $\alpha = 0$ the CAR and the proximity effect are induced and the MARS is absent. The situations at the DN/I/S junction interface are illustrated in Fig. 4. Here, it is important to note as follows: (i) It is valid for the restriction of only $\alpha = \pi/4$ in analysis for the circuit theory because the MARS channels quench the CAR and the proximity effect very effectively at $\alpha > 0.02\pi$ for the $d_{x^2-y^2}$-wave superconductor [28]. (ii) The CAR and the proximity effect cannot influence against junction properties in our fabricated junctions. The mesoscopic interference effect, such as the CAR and the proximity effect, must be negligible since our junction configuration satisfies $L \gg L_\phi$, where the length $L \simeq$ 1–2 mm mentioned in sec. 2 and the phase-breaking length $L_\phi \simeq$ 1–2 μm in Ag thin films at liquid-helium temperatures [75,76]. In this case, quasiparticles cannot interfere each other in the whole of the DN conductor on account of breaking the phase coherency between quasiparticles before phase coherent quasiparticles reach the Ag paste regarded as the reservoir [77].

As a result, the MARS channels sufficiently give influences in line shapes of $\sigma_{\rm T}(eV)$ rather than the CAR and the proximity effect in wide directions around $\alpha = \pi/4$, even if actual tunnel junctions slightly retain the surface roughness at the junction interface. Therefore, in analysis for around $\alpha = \pi/4$ corresponding to $\alpha \gg 0.02\pi$, those facts justify usage of a simplified formula for the circuit theory, just expressed by the Ohm's law: an elementary sum of $R_{R_{\rm d}=0}$ and $R_{\rm d}$ in a superconducting state. Without solving the Usadel equation in such a case, the normalized tunneling conductance $\sigma_{\rm T}(eV)$ can be approximated by the following simplified equations [30]:

$$\sigma_{\rm T}(eV) = \frac{\sigma_{\rm S}(eV)}{\sigma_{\rm N}(eV)} = \frac{R_{\rm b} + R_{\rm d}}{R_{R_{\rm d}=0} + R_{\rm d}}, \tag{1}$$

$$R_{R_{\rm d}=0} = \frac{R_{\rm b}}{\langle I_{\rm b0}\rangle}, \ \langle I_{\rm b0}\rangle = \frac{\langle I_{\rm b0}\rangle_{\rm S}}{\langle I_{\rm b0}\rangle_{\rm N}}, \tag{2}$$

$$\langle I_{\rm b0}\rangle_{\rm S} = \frac{1}{4k_{\rm B}T}\int_{-\infty}^{\infty} {\rm d}E \frac{1}{\pi}\int_{-\pi/2}^{\pi/2} {\rm d}\theta \ e^{-\lambda\theta^2} \times I_{\rm b0}\cos\theta \ {\rm sech}^2\left(\frac{E+eV}{2k_{\rm B}T}\right), \tag{3}$$

$$\langle I_{\rm b0}\rangle_{\rm N} = \frac{1}{4k_{\rm B}T}\int_{-\infty}^{\infty} {\rm d}E \frac{1}{\pi}\int_{-\pi/2}^{\pi/2} {\rm d}\theta \ e^{-\lambda\theta^2} \times T(\theta)\cos\theta \ {\rm sech}^2\left(\frac{E+eV}{2k_{\rm B}T}\right), \tag{4}$$

$$I_{\rm b0} = \frac{T(\theta)\left\{1 + T(\theta)|\Gamma_+|^2 + [T(\theta)-1]\,|\Gamma_+\Gamma_-|^2\right\}}{|1 + [T(\theta)-1]\,\Gamma_+\Gamma_-|^2}, \tag{5}$$

$$T(\theta) = \frac{4\cos^2\theta}{4\cos^2\theta + Z^2}, \tag{6}$$

$$\Gamma_+ = \frac{\Delta_+^*}{E + \sqrt{E^2 - \Delta_+^2}}, \ \Gamma_- = \frac{\Delta_-}{E + \sqrt{E^2 - \Delta_-^2}}, \tag{7}$$

with $\Delta_\pm = \Delta_0\cos[2(\theta \mp \alpha)]$, where Δ_0 denotes the maximum amplitude of the pair potential and θ is the injection angle of the quasiparticle measured from the x-axis. Here, an insulating barrier is expressed as a δ-function model $H\delta(x)$, where Z is an insulating barrier height given by $Z = 2mH/(\hbar^2 k_{\rm F})$ with Fermi momentum $k_{\rm F}$ and effective mass m. In the above equations, $k_{\rm B}$ is the Boltzmann's constant and the factor $\cos\theta$ is necessary for calculating a normal component relative to the junction interface of the tunneling current. Further λ is added in order to introduce the probability of tunneling directions at the junction interface, where we presume to be the Gauss distribution as a weight function.

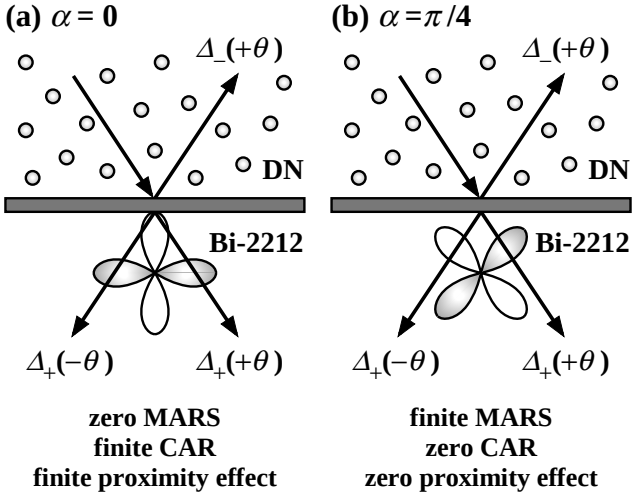

Fig. 4. Schematic illustrations of the junction interface: (a) $\alpha = 0$ and (b) $\alpha = \pi/4$. The trajectories in the scattering process for incoming and outgoing quasiparticles at the DN/I/S junction interface for d-wave superconductors and the corresponding pair potential $\Delta_\pm(\theta)$ are represented. We choose $\Delta_\pm = \Delta_0\cos[2(\theta \mp \alpha)]$ for the pairing symmetry of an order parameter because of the $d_{x^2-y^2}$-wave symmetry for Bi-2212 compounds. The our experimental condition corresponds to the case (b) for the situation at the junction interface.

The recent theoretical expectations of the circuit theory motivate us to analyze experimental ZBCP spectra in the ab-plane directions. For the circuit theory with the d-wave pairing symmetry, the theoretical results indicate that the ZBCP height is strongly reduced by taking into account the existence of the DN conductor, and the resulting $\sigma_{\rm T}(0)$ is not as high as that obtained in the ballistic regime [28,30]. One of the typical examples is plotted in Fig. 5. In the case of $\alpha = \pi/4$, the line shapes of $\sigma_{\rm T}(eV)$ are independent of $E_{\rm Th}$ because of the absence of the CAR and the proximity effect. The parameter values change only for $R_{\rm d}/R_{\rm b}$ in the tunneling spectral formula

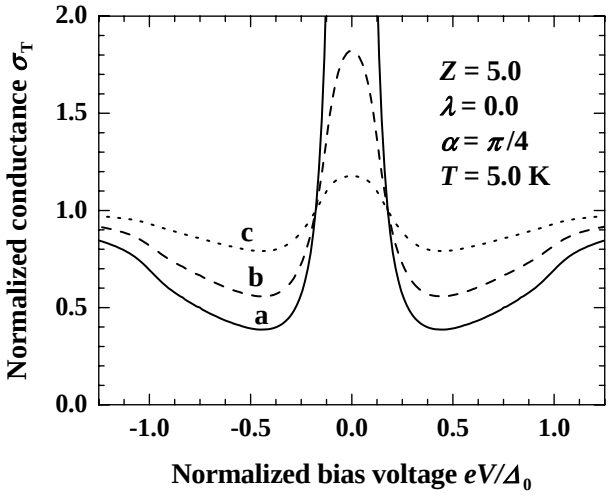

Fig. 5. Variations of the normalized tunneling conductance $\sigma_{\rm T}(eV)$ calculated by the circuit theory under the condition of $Z = 5.0$, $\lambda = 0.0$ and $\alpha = \pi/4$ at $T = 5.0$ K. a: $R_{\rm d}/R_{\rm b} = 0.0$, b: $R_{\rm d}/R_{\rm b} = 1.0$ and c: $R_{\rm d}/R_{\rm b} = 5.0$. It is important that the DN resistance $R_{\rm d}$ effectively suppresses the ZBCP height, but does not change the ZBCP width on the condition of $\alpha = \pi/4$ because the ZBCP comes from the formation of the MARS.

of eqs. (1)–(7). As shown in Fig. 5, the effect of $R_{\rm d}$ is obviously significant for the ZBCP height of the resulting $\sigma_{\rm T}(eV)$, but is independent of the ZBCP width of the resulting $\sigma_{\rm T}(eV)$. On the other hand, the ZBCP width is determined by an amplitude of Δ_0, Z and λ on the condition of $\alpha = \pi/4$. Figures 6 and 7 represent typical variations of line shapes of $\sigma_{\rm T}(eV)$ for Z and λ, respectively. Different from the case of $R_{\rm d}$ in Fig. 5, the height and width of the ZBCP change simultaneously with altering the value of Z or λ. Here, we note that for the circuit theory $R_{\rm b}$ depends

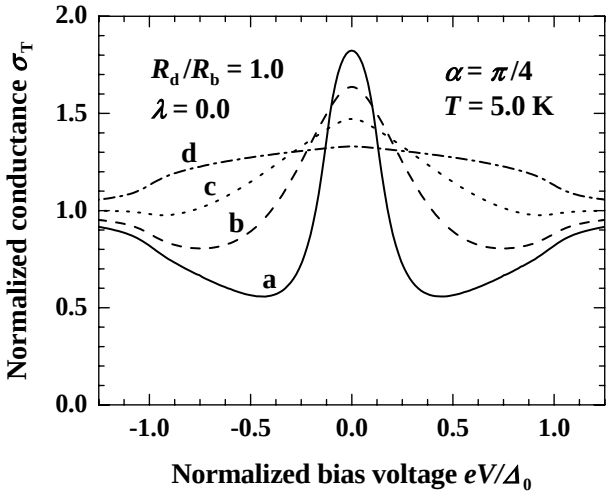

Fig. 6. Variations of the normalized tunneling conductance $\sigma_{\rm T}(eV)$ calculated by the circuit theory under the condition of $R_{\rm d}/R_{\rm b} = 1.0$, $\lambda = 0.0$ and $\alpha = \pi/4$ at $T = 5.0$ K. a: $Z = 5.0$, b: $Z = 2.0$, c: $Z = 1.0$ and d: $Z = 0.0$.

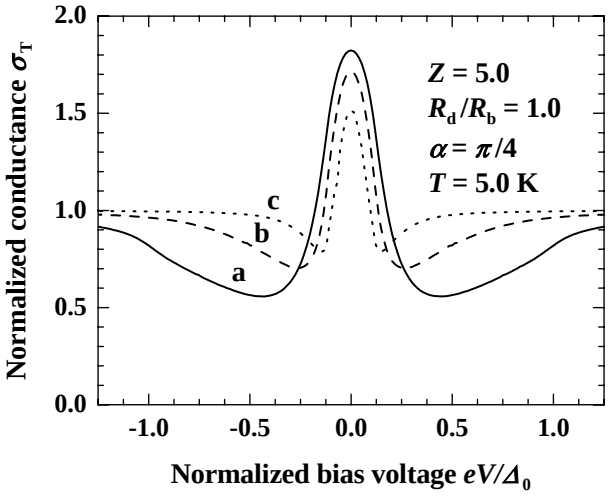

Fig. 7. Variations of the normalized tunneling conductance $\sigma_{\rm T}(eV)$ calculated by the circuit theory under the condition of $Z = 5.0$, $R_{\rm d}/R_{\rm b} = 1.0$ and $\alpha = \pi/4$ at $T = 5.0$ K. a: $\lambda = 0.0$, b: $\lambda = 10.0$ and c: $\lambda = 90.0$.

on Z by way of eq. (6) and the following equation [30]:

$$R_{\rm b} = \frac{2R_0}{\displaystyle\int_{-\pi/2}^{\pi/2} {\rm d}\theta\, T(\theta)\cos\theta}, \tag{8}$$

with Sharvin resistance R_0 at the junction interface. Therefore, for the actual quantitative comparison with tunneling experiments, these facts suggest that we must take into account the effect of $R_{\rm d}$. As shown in Fig. 2, the resulting ZBCP height from experiments is not as high as that obtained in the ballistic regime, so we can expect that the influence of $R_{\rm d}$ can replace that of Dynes's parameter Γ [57, 58] as a broadening factor in tunneling spectral formulas for the ZBCP. Therefore, we will analyze our experimental ZBCP results in terms of the circuit theory extended to the systems containing d-wave superconductor tunnel junctions.

3.3 Fitting results for the circuit theory

Figure 8 shows the spectral fit of the circuit theory for d-wave superconductors to our experimental data. In addition, in order to make a comparison between the circuit theory for DN/I/S tunnel junctions and the ballistic theory for N/I/S tunnel junctions, the fitting results for the ballistic theory are also given in Fig. 8 by calculating the equations cited in ref. [51]. The open circles represent the experimental data for the {110}-oriented tunnel junction in Fig. 2(c), normalized by a parabolic background. The solid line represents the fitting curve for the circuit theory extended to the systems containing d-wave superconductor tunnel junctions. The broken line represents that for the ballistic theory extended for d-wave superconductors, as well. The fitting results indicate good agreement between the experimental data and two theoretical curves.

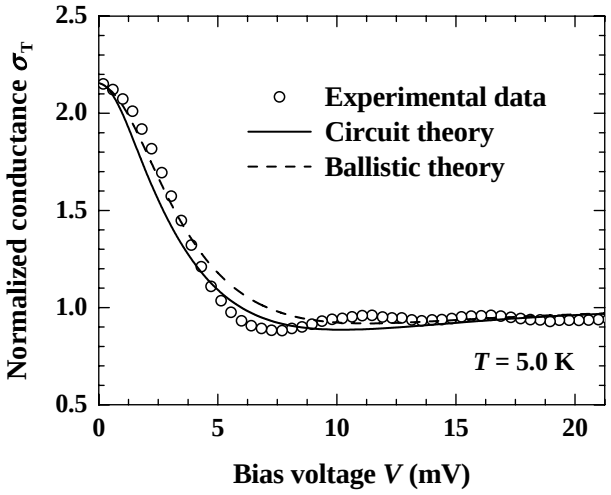

Fig. 8. Experimental tunneling spectrum at $T = 5.0$ K with the tunneling spectra of the circuit and ballistic theories for d-wave superconductors. The open circles represent the experimental result of the {110}-oriented junction for the Bi-2212 single crystal in Fig. 2(c). The experimental spectrum is normalized by a parabolic background. The solid line represents the tunneling spectrum calculated by the circuit theory extended to the d-wave pairing symmetry; and the broken line, that of the ballistic theory extended as well.

Other tunnel junctions of the same compound have been also studied in this fashion, and the results are very reproducible. The slight discrepancy between the experimental data and theoretical calculations in Fig. 8 seems to come from the simplification of the insulating barrier in the theories. Here, a junction interface between a superconducting state and a normal state is clearly defined, and a δ-function is used as a potential barrier. An actual tunnel junction is more complicated.

Table 1 denotes the corresponding parameter values in each theory. The difference in two fitting results is essentially recapitulated in values of Γ and $R_{\rm d}/R_{\rm b}$. Here, we emphasize that an introduction of the Dynes's parameter Γ in tunneling spectral formulas may not necessarily suggest the concrete smearing origin in experimental tunneling spectra in the case of (B) for the ballistic theory. On the other hand, in the analysis in the case of (A) for the circuit theory, the Dynes's parameter Γ as the broadening factor does not need to be introduced into the tunneling spectral formula because the resistance $R_{\rm d}$ of the DN conductor plays an important role as the suppression of the ZBCP height in tunneling conductance.

Here, we note several features for the fitting parameter values obtained from the circuit theory. The amplitude of $\Delta_0 = 25.0$ meV in the {110}-oriented direction is appropriate for comparison to ranges of roughly $\Delta_0 = 16$–40 meV for energy gap values in the {001}-oriented direction [78,79] and to the value of $\Delta_0 = 22.0$ meV obtained through the analysis of the {110}-oriented direction by using the ballistic theory in Table 1. Thus, for $2\Delta_0/k_{\rm B}T_{\rm c}$ a value of about 6.5 was obtained, typical

Table 1. Typical values of the fitting parameters in each tunneling conductance formula of (A) the circuit theory and (B) the ballistic theory, when compared to the experimental result for the {110}-oriented tunnel junction in Fig. 2(c). The "—" means that the parameter as $R_{\rm d}/R_{\rm b}$ does not exist in the spectral formula of the ballistic theory. It is important to note that, for the circuit theory, the Γ value as the broadening factor can equal to 0.0 meV, in spite of obtaining good fitting results.

	Δ_0 (meV)	Γ (meV)	Z	λ	$R_{\rm d}/R_{\rm b}$	α
(A)	25.0	0.0	2.2	13.0	0.35	$\pi/4$
(B)	22.0	1.7	2.3	13.0	—	$\pi/4$

for high-temperature superconductors [80]. The value of $Z = 2.2$ is comparatively small in variable ranges (see Fig. 10 in ref. [30]), so this result corresponds to relatively the low barrier height for our tunnel junctions. Corresponding to a finite value of Z, a finite potential height exists at the junction interface. Therefore, the tunneling directions of electrons and holes also restrict around normal to the junction interface. Consequently, the finite value of $\lambda = 13.0$ was obtained. Furthermore, we consider how the $\sigma_{\rm T}(eV)$ depends on the spread of $\boldsymbol{k}$-space in which tunneling electrons reach. The tunneling probability D as a function of the incident angle θ results in $D \propto \exp(-\lambda\theta^2)\cos\theta$ when $U \gg E_{\rm F}$, where U is the height of a tunneling barrier and $E_{\rm F}$ is Fermi energy [5]. The term $\exp(-\lambda\theta^2)\cos\theta$ is also contained in the equations cited in refs. [51,81]. As seen in Fig. 9, the directional dependence of tunneling probability becomes strong with increasing λ. When $\lambda = 0$, tunneling electrons range most in $\boldsymbol{k}$-space. On the other hand, when λ is enough large, electrons are restricted in the narrow region along an x-axis through the Γ point in the Brillouin zone. The planar type junction detects the electric state in narrow $\boldsymbol{k}$-space, while the

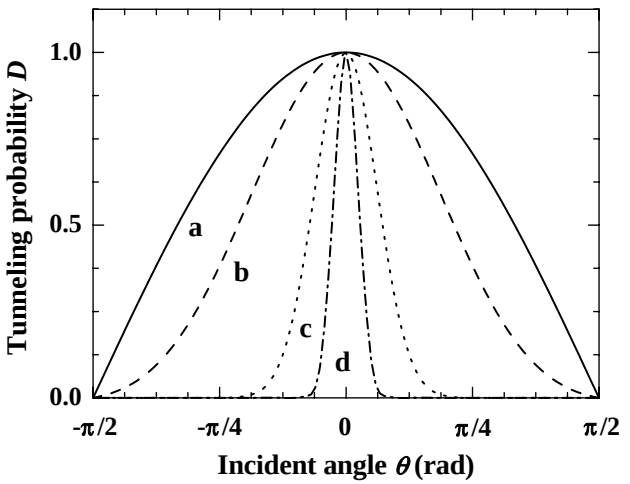

Fig. 9. Tunneling probability D as a function of incident angle θ for a: $\lambda = 0.0$, b: $\lambda = 1.0$, c: $\lambda = 13.0$ and d: $\lambda = 90.0$. The dotted line c is corresponding to the fitting results in both of the circuit theory and the ballistic theory in Fig. 8.

point contact spectroscopy and the STM/STS detect the electric state in wide $\boldsymbol{k}$-space. Therefore, it is reasonable that we have estimated $\lambda = 13.0$ as the parameter of the D from the analysis of the circuit theory for d-wave superconductors. Furthermore, the ratio of $R_{\rm d}/R_{\rm b} = 0.35$ may be not so large, but this value is sufficient to smear the spectral shape of the ZBCP by the influence of $R_{\rm d}$ in systems of d-wave superconductor tunnel junctions because the theoretical ZBCP height is effectively suppressed as shown in Fig. 5. As a result, in Fig. 8, we received good fitting results between the experimental ZBCP result in the {110}-oriented directions and the circuit theory. Hence, through analysis of the circuit theory, we are able not only to exclude the Dynes's parameter Γ from the tunneling spectral formula, but also able to obtain good fitting results of the ZBCP for the {110}-oriented tunnel junctions.

In this situation, we were successful in explaining the ZBCP behaviors by using the circuit theory for $\alpha = \pi/4$ including only the MARS and the influence of $R_{\rm d}$ in the tunneling spectral formula, in which the CAR and the proximity effect are completely suppressed. Other mechanisms may be responsible for the observed ZBCP smearing but the theoretical and quantitative estimates are certainly consistent with what we know about the DN resistance $R_{\rm d}$. We emphasize that it is appropriate for tunneling spectral formula to introduce the combined resistance for $R_{R_{\rm d}=0} + R_{\rm d}$, rather than the artificial smearing of Γ. It is suitable to understand that there is the relation between $R_{\rm d}$ and Γ. Namely, we can comprehend that finite lifetime of quasiparticles due to Dynes's parameter Γ arises from the scattering of quasiparticles at scatters in the DN conductor, which is expressed by $R_{\rm d}$ in eqs. (1)–(7) of the circuit theory. Thus, we can conclude that the effect of $R_{\rm d}$ plays an important role in tunneling spectra of high-$T_{\rm c}$ cuprate tunnel junctions as a new point of view for smearing origins in spectral shapes of the ZBCP. However, in order to progress further with analysis for the tunneling spectra in anisotropic superconductors, one must solve the Usadel equations, such as in ref. [30], for the quantitative discussions including much more general cases with arbitrary α values.

4 Conclusions

We have measured Ag–SiO–Bi-2212 planar tunnel junctions. The ZBCP enhancement was observed below $T_{\rm c}$ for the {110}-oriented tunnel junctions. Our experimental results for Ag–SiO–Bi-2212 planar tunnel junctions denote that Bi-2212 is obviously a d-wave superconductor and that the ZBCP originates from superconductivity. Hence, we have analyzed the ZBCP behaviors by using the circuit theory, which is constructed under the condition of the elementary sum of $R_{R_{\rm d}=0}$ and $R_{\rm d}$ at the DN/I/S junction interface for d-wave superconductors. The fitting results indicated good agreements between the experimental data and the theoretical curves not taking into account the Dynes's broadening factor Γ, in spite of the extreme case of $\alpha = \pi/4$ including only the influence of the MARS and $R_{\rm d}$ in the formula of tunneling conductance. As a new interpretation about smearing origins, the circuit theory gives that the smearing factor in tunneling spectra could be understood as the effect of the DN conductor in tunnel junctions, rather than that of Dynes's broadening parameter Γ. Thus, the circuit theory well describes the phenomena of quasiparticle tunnelings in anisotropic superconductors, rather than the ballistic theory, and such is very applicable to analysis of the actual experimental data of tunneling spectra of high-$T_{\rm c}$ cuprate tunnel junctions.

Acknowledgments

We would like to thank T. Arai, T. Uchida and Y. Tominari for supplying Bi-2212 single crystals. We appreciate T. Aomine, T. Fukami, S. W. M. Scott, S. Keenan and A. Odahara for helpful advice and discussions. We are additionally grateful to T. Asano for supporting SQUID measurements on some single crystals.

References

1. J. Lesueur, L. H. Greene, W. L. Feldmann, A. Inam, Physica C **191**, 325 (1992).
2. M. Taira, M. Suzuki, X.-G. Zheng, T. Hoshino, J. Phys. Soc. Jpn. **67**, 1732 (1998).
3. J. Y. T. Wei, N.-C. Yeh, D. F. Grarrigus, M. Strasik, Phys. Rev. Lett. **81**, 2542 (1998).
4. S. Kashiwaya, Y. Tanaka, Rep. Prog. Phys. **63**, 1641 (2000), and references therein.
5. A. Suzuki, M. Taira, M. Suzuki and X.-G. Zheng, J. Phys. Soc. Jpn. **70**, (2001) 3018.
6. Z. Q. Mao, K. D. Nelson, R. Jin, Y. Liu, Y. Maeno, Phys. Rev. Lett. **87**, 037003 (2001).
7. A. Sharoni, G. Koren, O. Millo, Europhys. Lett. **54**, 675 (2001).
8. T. Löfwander, V. S. Shumeiko, G. Wendin, Supercond. Sci. Technol. **14**, R53 (2001), and references therein.
9. I. Shigeta, F. Ichikawa, T. Aomine, Physica C **378-381**, 316 (2002).
10. M. Freamat, K.-W. Ng, Physica C **400**, 1 (2003).
11. Z. Q. Mao, M. M. Rosario, K. D. Nelson, K. Wu, I. G. Deac, P. Schiffer, Y. Liu, T. He, K. A. Regan, R. J. Cava, Phys. Rev. B **67**, 094502 (2003).
12. M. M. Qazilbash, A. Biswas, Y. Dagan, R. A. Ott, R. L. Greene, Phys. Rev. B **68**, 024502 (2003).
13. M. Freamat, K.-W. Ng, Phys. Rev. B **68**, 060507 (2003).
14. T. Miyake, T. Imaizumi, I. Iguchi, Phys. Rev. B **68**, 214520 (2003).
15. H. Kashiwaya, S. Kashiwaya, B. Prijamboedi, A. Sawa, I. Kurosawa, Y. Tanaka, I. Iguchi, Phys. Rev. B **70**, 094501 (2004).
16. M. Kawamura, H. Yaguchi, N. Kikugawa, Y. Maeno, H. Takayanagi, J. Phys. Soc. Jpn. **74**, 531 (2005).
17. G. Deutscher, Rev. Mod. Phys. **77**, 109 (2005), and references therein.
18. J. Appelbaum, Phys. Rev. Lett. **17**, 91 (1966).
19. P. W. Anderson, Phys. Rev. Lett. **17**, 95 (1966).
20. J. A. Appelbaum, Phys. Rev. **154**, 633 (1967).

21. S. C. Sanders, S. E. Russek, C. C. Clickner, J. W. Ekin, Appl. Phys. Lett. **65**, 2232 (1994).
22. M. Covington, R. Scheuerer, K. Bloom, L. H. Greene, Appl. Phys. Lett. **68**, 1717 (1996).
23. Y. Tanaka, S. Kashiwaya, Phys. Rev. Lett. **74**, 3451 (1995).
24. G. E. Blonder, M. Tinkham, T. M. Klapwijk, Phys. Rev. B **25**, 4515 (1982).
25. A. F. Volkov, A. V. Zaitsev, T. M. Klapwijk, Physica C **210**, 21 (1993).
26. Yu. V. Nazarov, Phys. Rev. Lett. **73**, 1420 (1994).
27. Yu. V. Nazarov, Superlattices Microstruct. **25**, 1221 (1999).
28. Y. Tanaka, Yu. V. Nazarov, S. Kashiwaya, Phys. Rev. Lett. **90**, 167003 (2003).
29. Y. Tanaka, A. A. Golubov, S. Kashiwaya, Phys. Rev. B **68**, 054513 (2003).
30. Y. Tanaka, Yu. V. Nazarov, A. A. Golubov, S. Kashiwaya, Phys. Rev. B **69**, 144519 (2004); Y. Tanaka, Yu. V. Nazarov, A. A. Golubov, S. Kashiwaya, *ibid.* **70**, 219907(E) (2004).
31. Y. Tanaka, S. Kashiwaya, Phys. Rev. B **70**, 012507 (2004).
32. T. Yokoyama, Y. Tanaka, A. A. Golubov, J. Inoue, Y. Asano, Phys. Rev. B **72**, 094506 (2005).
33. Y. Tanaka, Y. Asano, A. A. Golubov, S. Kashiwaya, Phys. Rev. B **72**, 140503 (2005).
34. T. Yokoyama, Y. Tanaka, A. A. Golubov, Y. Asano, Phys. Rev. B **72**, 214513 (2005).
35. I. Asulin, A. Sharoni, O. Yulli, G. Koren, O. Millo, Phys. Rev. Lett. **93**, 157001 (2004).
36. A. Sharoni, I. Asulin, G. Koren, O. Millo, Phys. Rev. Lett. **92**, 017003 (2004).
37. S. H. Pan, E. W. Hudson, K. M. Lang, H. Eisaki, S. Uchida, J. C. Davis, Nature **403**, 746 (2000).
38. K. M. Lang, V. Madhavan, J. E. Hoffman, E. W. Hudson, H. Eisaki, S. Uchida, J. C. Davis, Nature **415**, 412 (2002).
39. K. McElroy, R. W. Simmonds, J. E. Hoffman, D.-H. Lee, J. Orenstein, H. Eisaki, S. Uchida, J. C. Davis, Nature **422**, 592 (2003).
40. M. Vershinin, S. Misra, S. Ono, Y. Abe, Y. Ando, A. Yazdani, Science **303**, 1995 (2004).
41. T. Hanaguri, C. Lupien, Y. Kohsaka, D.-H. Lee, M. Azuma, M. Takano, H. Takagi, J. C. Davis, Nature **430**, 1001 (2004).
42. K. McElroy, J. Lee, J. A. Slezak, D.-H. Lee, H. Eisaki, S. Uchida, J. C. Davis, Science **309**, 1048 (2005).
43. M. Aprili, M. Covington, E. Paraoanu, B. Niedermeier, L. H. Greene, Phys. Rev. B **57**, R8139 (1998).
44. M. Aprili, E. Badica, L. H. Greene, Phys. Rev. Lett. **83**, 4630 (1999).
45. W. Wang, M. Yamazaki, K. Lee, I. Iguchi, Phys. Rev. B **60**, 4272 (1999).
46. A. Sharoni, O. Millo, A. Kohen, Y. Dagan, R. Beck, G. Deutscher, G. Koren, Phys. Rev. B **65**, 134526 (2002).
47. I. Iguchi, W. Wang, M. Yamazaki, Y. Tanaka, S. Kashiwaya, Phys. Rev. B **62**, R6131 (2000).
48. M. Sato, Physica C **263**, 271 (1996).
49. Y. Idemoto, K. Fueki, Jpn. J. Appl. Phys. **29**, 2729 (1990).
50. A. Yamamoto, M. Onoda, E. Takayama-Muromachi, F. Izumi, T. Ishigaki, H. Asano, Phys. Rev. B **42**, 4228 (1990).
51. I. Shigeta, T. Uchida, Y. Tominari, T. Arai, F. Ichikawa, T. Fukami, T. Aomine, V. M. Svistunov, J. Phys. Soc. Jpn. **69**, 2743 (2000).
52. S. Sinha, K.-W. Ng, Phys. Rev. Lett. **80**, 1296 (1998).
53. S. Sinha, K.-W. Ng, J. Phys. Chem. Solids **59**, 2078 (1998).
54. M. Covington, M. Aprili, E. Paraoanu, L. H. Greene, F. Hu, J. Zhu, C. A. Mirkin, Phys. Rev. Lett. **79**, 277 (1997).
55. Y Tanaka, Y. Tanuma, K. Kuroki, S. Kashiwaya, J. Phys. Soc. Jpn. **71**, 2102 (2002).
56. N. Kitaura, H. Itoh, Y. Asano, Y. Tanaka, J. Inoue, Y. Tanuma, S. Kashiwaya, J. Phys. Soc. Jpn. **72**, 1718 (2003).
57. R. C. Dynes, V. Narayanamurti, J. P. Garno, Phys. Rev. Lett. **41**, 1509 (1978).
58. R. C. Dynes, J. P. Garno, G. B. Hertel, T. P. Orlando, Phys. Rev. Lett. **53**, 2437 (1984).
59. M. Suzuki, K. Komorita, M. Nagano, J. Phys. Soc. Jpn. **63**, 1449 (1994).
60. S. Tanaka, E. Ueda, M. Sato, K. Tamasaku, S. Uchida, J. Phys. Soc. Jpn. **65**, 2212 (1996).
61. L. Alff, H. Takashima, S. Kashiwaya, N. Terada, H. Ihara, Y. Tanaka, M. Koyanagi, K. Kajimura, Phys. Rev. B **55**, R14757 (1997).
62. S. Kashiwaya, T. Ito, K. Oka, S. Ueno, H. Takashima, M. Koyanagi, Y. Tanaka, K. Kajimura, Phys. Rev. B **57**, 8680 (1998).
63. T. Cren, D. Roditchev, W. Sacks, J. Klein, Europhys. Lett. **52**, 203 (2000).
64. R. S. Gonnelli, A. Calzolari, D. Daghero, L. Natale, G. A. Ummarino, V. A. Stepanov, M. Ferretti, Eur. Phys. J. B **22**, 411 (2001).
65. T. Imaizumi, T. Kawai, T. Uchiyama, I. Iguchi, Phys. Rev. Lett. **89**, 017005 (2002).
66. H. Schmidt, J. F. Zasadzinski, K. E. Gray, D. G. Hinks, Phys. Rev. Lett. **88**, 127002 (2002).
67. A. Kohen, G. Leibovitch, G. Deutscher, Phys. Rev. Lett. **90**, 207005 (2003).
68. B. W. Hoogenboom, C. Berthod, M. Peter, Ø. Fischer, A. A. Kordyuk, Phys. Rev. B **67**, 224502 (2003).
69. T. Takasaki, T. Ekino, T. Muranaka, T. Ichikawa, H. Fujii, J. Akimitsu, J. Phys. Soc. Jpn. **73**, 1902 (2004).
70. H. Ding, M. R. Norman, J. C. Campuzano, M. Randeria, A. F. Bellman, T. Yokoya, T. Takahashi, T. Mochiku, K. Kadowaki, Phys. Rev. B **54**, R9678 (1996-II).
71. Y. Itoh, K. Yoshimura, T. Ohomura, H. Yasuoka, Y. Ueda, K. Kosuge, J. Phys. Soc. Jpn. **63**, 1455 (1994).
72. P. Bourges, L. P. Regnault, Y. Sidis, C. Vettier, Phys. Rev. B **53**, 876 (1996-II).
73. C. Panagopoulos, T. Xiang, Phys. Rev. Lett. **81**, 2336 (1998).
74. D. A. Wollman, D. J. Van Harlingen, W. C. Lee, D. M. Ginsberg, A. J. Leggett, Phys. Rev. Lett. **71**, 2134 (1993).
75. V. T. Petrashov, V. N. Antonov, P. Delsing, R. Claeson, Phys. Rev. Lett. **70**, 347 (1993).
76. V. T. Petrashov, V. N. Antonov, P. Delsing, T. Claeson, Phys. Rev. Lett. **74**, 5268 (1995).
77. B. J. van Wees, P. de Vries, P. Magnée, T. M. Klapwijk, Phys. Rev. Lett. **69**, 510 (1992).
78. Q. Huang, J. F. Zasadzinski, K. E. Gray, J. Z. Liu, H. Claus, Phys. Rev. B **40**, 9366 (1989).
79. N. Miyakawa, J. F. Zasadzinski, L. Ozyuzer, P. Guptasarma, D. G. Hinks, C. Kendziora, K. E. Gray, Phys. Rev. Lett. **83**, 1018 (1999).
80. K. Kitazawa, H. Sugawara, T. Hasegawa, Physica C **263**, 214 (1996).
81. S. Kashiwaya,Y. Tanaka, M. Koyanagi, H. Takashima, K. Kajimura, Phys. Rev. B **51**, 1350 (1995); S. Kashiwaya, Y. Tanaka, M. Koyanagi, K. Kajimura, *ibid.* **53**, 2667 (1996).